EBioMedicine 53 (2020) 102695

Contents lists available at ScienceDirect

EBioMedicine

journal homepage: www.elsevier.com/locate/ebiom

Research paper

Elevated myocardial SORBS2 and the underlying implications in left ventricular noncompaction cardiomyopathy

Chunyan Li[a], Fan Liu[b], Shenghua Liu[a], Haizhou Pan[c], Haiwei Du[a], Jian Huang[a], Yuanyuan Xie[a], Yanfen Li[a], Ranxu Zhao[a], Yingjie Wei[a,*]

[a] State Key Laboratory of Cardiovascular Disease, Fuwai Hospital, National Center for Cardiovascular Diseases, Chinese Academy of Medical Sciences and Peking Union Medical College, 167 Beilishi Road, Beijing 100037, China
[b] Department of Human Anatomy, Histology and Embryology, Institute of Basic Medical Sciences, Chinese Academy of Medical Sciences, School of Basic Medicine, Peking Union Medical College, Beijing, China
[c] Children's Heart Center, the Second Affiliated Hospital and Yuying Children's Hospital, Institute of Cardiovascular Development and Translational Medicine, Wenzhou Medical University, Wenzhou, Zhejiang, China

ARTICLE INFO

Article History:
Received 21 November 2019
Revised 11 February 2020
Accepted 12 February 2020
Available online xxx

Keywords:
LVNC
SORBS2
Microtubule
Junctophilin-2
Heart failure

ABSTRACT

Background: Left ventricular noncompaction cardiomyopathy (LVNC) is a hereditary heart disease characterized by an excessive trabecular meshwork of deep intertrabecular recesses within the ventricular myocardium. The guidelines for management of LVNC patients aim to improve quality of life by preventing cardiac heart failure. However, the mechanism underlying LVNC-associated heart failure remains poorly understood.
Methods: Using protein mass spectrometry analysis, we established that Sorbin And SH3 Domain Containing 2 (SORBS2) is up-regulated in LVNC hearts without changes to structure proteins. We conducted *in vivo* experiments wherein the heart tissues of wild-type mice were injected with an AAV9 vector to overexpress SORBS2, followed by analysis using echocardiography, T-tubule analysis and Ca^{2+} imaging to identify functional and morphological changes. In addition, we analyzed the function and structure of SORBS2 overexpressing human embryonic stem cell (hESC) derived cardiomyocytes (hESC-CM) via immunoblotting, immunohistochemistry, immunofluorescence, and confocal Ca^{2+} imaging.
Findings: LVNC myocardial tissues feature strongly elevated expression of SORBS2, microtubule densification and redistribution of Junctophilin 2 (JP2). SORBS2 interacts with β-tubulin, promoting its polymerization in 293T cells and hESC-derived CMs. *In vivo*, cardiac dysfunction, β-tubulin densification, JP2 translocation, T-tubule disorganization and Ca^{2+} handling dysfunction were observed in mice overexpressing SORBS2.
Interpretation: We identified a novel mechanism through which SORBS2 interacts with β-tubulin and promotes microtubule densification, eventually effecting JP2 distribution and T-tubule, potentially contributing to heart failure in LVNC disease.
Fund: This work was supported by a CAMS Initiative for Innovative Medicine grant (CAMS-I2M, 2016-I2M-1-015 to Y.J.Wei)

1. Introduction

Left ventricular noncompaction cardiomyopathy (LVNC) is currently classified as a clinically heterogeneous primary genetic cardiomyopathy by the American Heart Association: characterized by an excessive trabecular meshwork of deep intertrabecular recesses within the ventricular myocardium [1]. The most common clinical presentations of LVNC are congestive heart failure, cardiac arrhythmia, and thromboembolism [1,2]. However, the underlying mechanisms driving cardiac dysfunction in LVNC remain largely unknown.

Sorbin and SH3 Domain Containing 2 (SORBS2) is a member of the SOHO protein family and is highly expressed in the myocardium, with known localization in Z-bands and in intercalated discs

Abbreviation: LVNC, left ventricular noncompaction cardiomyopathy; ARVC, arrhythmogenic right ventricular cardiomyopathy; HCM, hypertrophic cardiomyopathy; NC, normal control; JP2, junctophilin 2; SORBS2, sorbin and SH3 domain containing 2; OCD, oriented cell division; LV, left ventricular; E-C coupling, excitation-contraction coupling; RyR2, type two ryanodine receptor; SR, Sarcoplasmic reticulum; Co-IP, Co-immunoprecipitation; SORBS2-OE, Overexpression of the SORBS2; HPLC, High-performance liquid chromatography; hESC CMs, Human embryonic stem cell (hESC) derived cardiomyocytes; AAV9, Adeno-associated virus; AGC, Automatic gain control; CID, Collision-induced dissociation

* Corresponding author.
E-mail address: weiyingjie@fuwaihospital.org (Y. Wei).

https://doi.org/10.1016/j.ebiom.2020.102695

Research in context

Evidence before this study

Left ventricular noncompaction cardiomyopathy (LVNC) is a clinically heterogeneous primary genetic cardiomyopathy, but the underlying mechanisms for the development and progression of heart failure in LVNC remains unclear. Sorbin and SH3 domain-containing protein 2 (SORBS2) is known to be localized at the Z-bands and intercalated disks in cultured cardiomyocytes, but there are no previous reports associated SORBS2 with LVNC.

Added value of this study

Our results obtained from an initial proteomics-based study of human heart tissues from transplant patients and subsequent follow-up experiments establish that SORBS2 interacts with β-tubulin and promotes microtubule densification, that elevated SORBS2 levels substantially disrupt cardio-mechanical function, and that dysregulated SORBS2 accumulation disrupts the spatial organization and perhaps E-C junction related function of JP2. Medically, it is possible that SORBS2 may have diagnostic value for the early detection or ongoing management of heart diseases.

Implications of all the available evidence

Our study demonstrates a pathogenic contribution of elevated SORBS2 levels in LVNC and highlights how increased SORBS2 affects multiple cellular and physiological processes in heart tissues. Thus, beyond revealing a previously unknown contribution of SORBS2 in the etiopathogenesis of LVNC, our study provides basic insights about the biological function of SORBS2 which suggest potential therapeutic strategies for the detection, treatment, and management of LVNC.

(Fig. S1a) of mature myofibrils in healthy individuals [3]. SORBS2 is functions as a scaffold protein that coordinates multiple signaling pathways converging on the actin and microtubule cytoskeleton [4]. Overexpression of SORBS2 can account for the defects in cytoskeleton dynamics and increased actomyosin cell contractility, and is correlated with destabilization of the microtubule network [4]. Tubulin polymerization or depolymerization regulates multiple processes which are required for trabecular initiation and formation, including specifying the polarity of the myocardium [5], oriented cell division (OCD) [6], and directional migration of the cardiomyocytes [7].

Microtubule over densification was found to be inversely related with left ventricular (LV) fractional shortening [8,9]. Microtubule densification is a commonly observed in multiple animal models of cardiac disease [10,11], and it has been suggested that increased β-tubulin protein levels contribute to cardiac dysfunction [12]. Multiple lines of evidence suggest that an increased density of β-tubulin protein in the left ventricle can lead to pressure overload, and it has been demonstrated that excess polymerization of β-tubulin undermines contractility in cardiomyocytes [13,14]. It is also known that tubulin expression levels are increased in human hypertrophied and failing myocardia. However, the mechanism through which microtubule densification deleteriously affects cardiac function remains poorly understood [15,16].

Junctophilin-2 (JP2), a member of the junctophilin protein family, plays an important role in the formation and maintenance of the cardiac dyad microdomain [17,18]. Previous studies have indicated that reduction of junctophilin protein expression levels sustain structural and functional consequences, and recent study reported JP2 redistribution as a novel mechanism for loss of Excitation-contraction coupling (E-C coupling) and heart failure [13,14]. Regular heart contraction critically depends on precisely-controlled cytosolic Ca^{2+} regulation during each cardiac cycle [19]. Similarly, contraction is mainly driven by Ca^{2+} ions released from the sarcoplasmic reticulum (SR), which plays a particularly important role in activation of myocyte contraction [14]. As the major SR Ca^{2+} release channel in ventricular myocytes, the type 2 ryanodine receptor (RyR2) is essential for rapid electrical excitation, initiation and synchronous triggering of SR Ca^{2+} release, thereby coordinating myocyte contraction [20,21].

The present study adopted a proteomics approach to assess human heart tissues from patients with heart failure, and identified that elevated SORBS2 levels in LVNC patients contribute to multiple cellular and pathophysiological processes in heart tissues in humans and in mice.

2. Materials and methods

2.1. Patients

Seven normal control hearts (NC, n = 7) were harvested from autopsies or donors with no history of heart disease who died in accidents. The 23 myocardial samples, including LVNC, ARVC, and HCM patients, were taken from our heart transplantation program. Left ventricular (LV) samples were obtained from 23 patients with chronic heart failure due to left ventricular noncompaction (LVNC, n = 8), arrhythmogenic right ventricular cardiomyopathy (ARVC, n = 8), and hypertrophic cardiomyopathy (HCM, n = 7) undergoing heart transplantation, and seven control subjects from autopsies or donors with no history of heart disease who died in accidents. All participants gave informed written consent for this investigation, which was approved by the Institutional Ethical Review Board of Fuwai Hospital (Beijing, China), and conformed to the principles outlined in the Declaration of Helsinki. The basic characteristics of patients are shown in Table S1.

2.2. Proteomics

2.2.1. Protein extraction and digestion

Each of the frozen ventricular tissue samples was ground into a powder using liquid nitrogen and then transferred to a 5-mL centrifuge tube. Subsequently, four volumes of lysis buffer (8 M urea, 1% Protease Inhibitor Cocktail) was added to the cell powder, followed by sonication (three times) on ice using a high intensity ultrasonic processor (Scientz). The remaining debris was removed by centrifugation at 12,000 x g at 4 °C for 10 min. Finally, the supernatant was collected and the protein concentration was determined through a BCA kit (supplier) according to the manufacturer's instructions. The protein solution was reduced with 5 mM dithiothreitol for 30 min at 56 °C and alkylated with 11 mM iodoacetamide for 15 min at room temperature in darkness. The protein sample was then diluted by adding 100 mM TEAB to urea concentration < 2 M. Finally, trypsin was added at 1:50 trypsin-to-protein mass ratio for the first digestion overnight and 1:100 trypsin-to-protein mass ratio for a second 4 h digestion.

2.2.2. TMT labeling

After trypsin digestion, peptides were desalted using a Strata X C18 SPE column (Phenomenex), followed by vacuum-drying. Peptides were reconstituted in 0.5 M TEAB and processed according to the manufacturer's protocol for a TMT kit. Briefly, one unit of TMT reagent was thawed and reconstituted in acetonitrile. The peptide mixtures were then incubated for 2 h at room temperature and pooled, desalted and dried by vacuum centrifugation.

2.2.3. Two-dimensional liquid chromatography-tandem mass spectrometry (2D LC-MS/MS)

The TMT samples were initially separated in one dimensional via high-pH reverse phase high-performance liquid chromatography (HPLC) system (Rigol, L-3120, Beijng, China) [22]. The peptide samples were loaded onto a Durashell C18 column (150 Å, 5 μm, 4.6 × 250 mm,

Agela, Wilmington, DE, USA) with solvent Buffer A (2% ACN and 98% ddH_2O, pH=10, adjusted with ammonium hydroxide) and eluted with Buffer B (98% ACN and 2% ddH_2O, pH=10, adjusted with ammonium hydroxide) using the following separation gradient: 0%−3% B, 8 min; 3%−22% B, 37 min; 22%−32% B, 10 min; 32%−90% B, 1 min; 90% B, 2 min; 90%−0% B, 2 min. The column oven was set at 45 °C and the peptides were separated at an eluent flow rate of 700 μl/min and monitored by UV detection at 214 nm. The second dimension of the separation was reverse phase chromatography analysis using an EASY-nLC 1200 ultra-high-pressure system (Thermo Fisher Scientific, Waltham, MA, USA), which was coupled to an Orbitrap Fusion Lumos Mass Spectrometer (Themo Fisher Scientific, Waltham, MA, USA) interfaced with a electrospray ion source. Chromatography was performed using a 16-cm long silica capillary column (75 μm inner diameter) packed in house with 3 μm resins (Dr. Maisch GmbH reversed-phase material Reprosil-Pur 120 C18-AQ) (SinoAmerican Proteomics LLC). The peptides were loaded onto a trap column at 10 μl/min with solvent A (2% ACN and 0.1% FA in ddH_2O, pH=2.7) for 1 min and eluted with a linear 75-min gradient of 3%−42% solvent B (99.9% ACN and 0.1% FA) at a flow rate of 300 nL/min. After each gradient, the column was flushed with 95% solvent B for another 10 min. For MS data acquisition, the eluted peptides were ionized under high voltage (2.0 KV) using an Orbitrap Fusion Lumos Mass Spectrometer (Themo Fisher Scientific, Waltham, MA, USA), which was operated in data-dependent mode. In each cycle, a full scan was acquired at a resolution of 60,000 in a survey scan (350−1500 m/z) with an automatic gain control (AGC) target value of 2 × 106 ions. The ten most intense precursor ions were sequentially fragmented by alternating collision-induced dissociation (CID) and higher energy collision induced dissociation (HCD) fragmentation.

2.2.4. Data processing, protein identification and deposition in a public database

The acquired LC-MS/MS raw data were analyzed with Proteome Discoverer software (Version2.1, Thermo Fisher Scientific, Waltham, MA, USA) against the UniProtKB/Swiss-Prot and UniProtKB/VarSplic human reference protein databases. Search parameters used were as follows: precursor ion mass tolerance: ± 20 ppm, daughter ion (MS^2 fragment ion) mass tolerance: 0.02 Da; granddaughter ion (MS^3 fragment ion) mass tolerance: ± 10 ppm; enzyme: trypsin; two missing cleavages were allowed; fixed modification: carbamidomethylation (C); dynamic modification: oxidation (M) and quantitative measurement: TMT MS^3. A target-decoy search strategy was applied for controlling the false discovery rate (FDR) of peptides and proteins. The data for the proteomics experiments has been deposited at Mendeley Data, a platform for sharing citable research datasets online: Mass Spectrometry DOI: 10.17632/v3k385htnt.1

2.3. Western blotting

The heart tissues and cells were harvested and washed twice with PBS and then lysed with cool RIPA and centrifuged at 12,000xg at 4 °C for 10 min. The supernatants were collected and assayed via BCA protein assay kit. The tissues and cell homogenates were separated by SDS-PAGE (4%−12% gradient) and transferred to PVDF membranes. The PVDF membranes were blocked by TBS-T with 5% milk for 2 h, subsequently incubated with primary antibodies overnight at 4 °C and incubated with secondary HRP-IgG antibodies (CST Biotechnology) for 2 h at RT. The primary antibodies used were as follows: rabbit polyclonal anti-SORBS2 (1:1000; Proteintech); mouse monoclonal anti-GAPDH (1:1000; Proteintech); mouse and rabbit monoclonal anti-β-tubulin (1:1000; CST); mouse monoclonal anti-a-tubulin (1:1000; Proteintech); rabbit polyclonal anti-RyR2 (1:1000; Invitrogen); rabbit polyclonal anti-JP2 (1:1000; Abcam); rabbit monoclonal anti-flag (1:1000; CST);

2.4. Co-immunoprecipitation

Co-IP assays were carried out by the (88,804 Pierce Classic Magnetic IP/Co-IP Kit, Thermo). The antibodies used are as follows: IP: rabbit polyclonal anti-SORBS2 (2 μg; Proteintech); rabbit monoclonal anti-β-tubulin (2 μg; Proteintech); IB: rabbit polyclonal anti-SORBS2 (1:1000; Proteintech); rabbit monoclonal anti-β-tubulin (1:1000; CST); Heart tissues were lysed in ice-cold lysis buffer. Extracted proteins were collected via centrifugation at 12 000 rpm for 10 min at 4 °C. The lysates were then incubated with 5 μg of antibodies pre-bound to protein A/G-sepharose beads overnight at 4 °C. Beads were washed four times with ice-cold washing buffer, eluted in SDS-PAGE sample repeat (50 mM Tris−HCl (pH 6.8), 2% SDS, 0.1% bromophenol blue, 10% glycerol, 10 mM dithiothreitol). The precipitates were subjected to immunoblotting with antibodies.

2.5. Extraction of samples

The samples (human heart tissues and cell samples) were homogenized in a microtubule stabilization buffer with protease and phosphatase inhibitor cocktails to inhibit the degradation [23,24] (1% Nonidet P-40, 50% glycerol, 5% Me_2SO, 0.5 mm GTP, 10 mm Na_2HPO_4, 0.5 mm EGTA, 0.5 mm $MgSO_4$, 25 mm $Na_4P_2O_7$). And then they the lysate was centrifuged at 100,000 × g at 25 °C for about 30 min. This supernatant was saved as the tubulin heterodimer fraction (free tubulin), and the pellet was resuspended in 1% SDS buffer and boiled for 5 min to dissolve which was saved as the microtubule fraction (polymerized tubulin). The tubulin heterodimer and microtubule fractions were each mixed with an equal volume of SDS sample buffer and boiled for 3 min. Samples are ready for gel electrophoresis.

2.6. Immunofluorescence and immunohistochemistry

Cells were cultured on glass coverslips with gelatin, fixed for 15 min in cold 4% paraformaldehyde, then washed with PBS for 10 min, incubated with 5% normal goat serum (NGS; ZSGB-BIO, Beijing, China) in PBS for one hour at RT, then washed with PBS for 10 min, followed by incubation with the primary antibody overnight at 4 °C and then washed with PBS for 10 min. The cells were incubated with IgG peroxidase-conjugated secondary antibody for 1 h and washed with PBS for 10 min, followed by observation with a Leica Sp8 confocal scanning laser microscope (Sp8; Leica). The immunohistochemistry procedure was similar to that described above. The myocardial samples were fixed in 10% neutral buffered formalin. After paraffin embedding, a series of alcohol and xylene gradients were used for dehydration, followed by blocking with 0.05% H_2O_2. Immunohistochemistry images were acquired using a Leica DM750 microscope (magnification 400 ×).

2.6.1. The antibodies and dilutions used were as follows

Rabbit anti-SORBS2 (1:100; Proteintech) and mouse anti-Sarcomeric Alpha Actinin (1:100, Abcam);mouse and rabbit monoclonal anti-β-tubulin (1:100; CST); rabbit polyclonal anti-RyR2 (1:200; Invitrogen); rabbit polyclonal anti-JP2 (1:100; Abcam); rabbit polyclonal anti-Nanog (1:200;CST); rabbit monoclonal anti-Oct4A (1:100;CST); rabbit polyclonal anti-MLC-2V (1:100; proteintech); rabbit polyclonal anti-CTNI (1:100; Proteintech); rabbit polyclonal anti-CTNT (1:100; Proteintech); rabbit polyclonal anti-Sox2 (1:100; CST); rabbit polyclonal anti-SSEA (1:100; CST); Alexa 488-conjugated goat anti-mouse (Yeasen Biology); Alexa 594-conjugated goat anti-rabbit (Yeasen Biology). The cell nuclei were counterstained with 0.1% 4′, 6-diamidino-2-phenylindole (DAPI).

2.7. Wheat germ agglutinin (WGA) staining

After blocking with 1% bovine serum albumin (BSA), tissue sections were incubated with wheat germ agglutinin Alexa Fluor 488 (1:200) for 2 h in room temperature. After washing three times with

PBS, the slides were mounted with a mounting medium. Stained cells were visualized using a fluorescence microscope.

2.8. Cell culture and transfection

The cell culture experiments followed standard protocols. Briefly, human embryonic stem cells were cultured in TeSR™-E8™ Basal Medium supplemented with TeSR™-E8™ media (StemCell Technologies, Cat. # 05990). Once the stem cells reached 70% confluency, they were then prepared to induce hESC-CMs. RPMI1640 containing 3 μM CHIR-99021HCl (Selleck Chem, Cat. # S2924), and 2% B-27 minus insulin (Gibco) as the culture media to induce hESCs. After 3 days, the cells were cultured in RPMI1640 containing 5 μM IWR-1-endo (Selleck Chem, S7086) and 2% B-27 minus insulin (Gibco). Two days later, the media was replaced with RPMI1640 containing 2% B-27 minus insulin (Gibco). RPMI1640 plus 1 × B-27 supplement was given, and on day 16, collagenase type I (Sigma) was used to purify the cells, and these were then cultured in Dulbecco's Modified Eagle's Medium supplemented with 15% fetal bovine serum (Gibco) at 37 °C and 5% CO_2 in a humidified incubator. In order to evaluate the function of SORBS2 in cardiomyocytes, we generated HBLV-GFP-PURO-NC and HBLV-h-3*flag-GFP-SORBS2 constructs to disrupt the cardiomyocytes and performed lentiviral (HANBIO) transfection after the hESC-CMs confluence reached nearly 70%, and a density of 1×10^6 virions in each well of a 6-well plate. After transfection for 48 h, green fluorescence intensity could be observed under a fluorescence microscope (Leica DM750).

2.9. Calcium imaging in hESC-CMs

Intracellular calcium imaging was performed as previously described [25]. Briefly, hESC-CMs were treated with 2 μM Fura-2AM (Fura-2 acetoxymethyl ester fura-2 AM-acetoxy-methyl ester) and cells were incubated for about 30 min at 37 °C in a dark room. After washing with HEPES, glass coverslips were placed on the recording chamber with HEPES buffer at a flow rate of 1.5 ml/min at room temperature. Images were recorded using an upright NIKON ECLIPSE Ti microscope equipped with a ratio metric imaging system (Nikon NIS-Elements AR 4.00.00). The ratio of 340 nm/380 nm fluorescence intensity (R340/380) within a certain region of interest after background subtraction was used as a relative measure of intracellular calcium concentration ($[Ca^{2+}]i$) [26]. Calibration with external standards (Calcium Calibration Buffer Kit, Invitrogen) showed that R340/380 increased linearly with $[Ca^{2+}]i$ up to about 1 lM and R340/380 of 0.7−1.25 corresponded to basal $[Ca^{2+}]i$ of 90−180 nM. Therefore, the hESC-CMs with R340/380 in the range 0.7−1.25 were included in this study. All reagents were dissolved in HEPES buffer and applied locally to the hESC-CMs through a micropipette (with a tip diameter of 100 μm) and an 8-channel pressure-controlled drug application system (VC3-8PP, ALA Scientific).

2.10. Calcium imaging in isolated cardiomyocytes

Cultured cardiomyocytes were loaded with 5 μmol/L Fluo-4 AM (Invitrogen, Grand Island, NY) in 1.8 mmol/L Ca^{2+}Tyrode solution for 30 min. Cells were then washed with dye-free Tyrode solution for 20 min for de-esterification before imaging. The Ca^{2+} images were acquired using confocal microscopy in line−scan mode along the longitudinal axis of myocytes. Steady-state Ca^{2+} transients were measured in Tyrode's solution containing 1.8 mmol/L Ca^{2+} under field stimulation of 1 Hz.

2.11. Impedance

All hESC-CMs used in this study were monitored during spontaneous beating. We used 50,000 cells per well on a cardioexcyte 96 sensor plate according to cell manufacturer recommendations. Prior to compound application, all hESC-CMs cells formed syncytial monolayers that were suitable for electrophysiological and phenotypical assessments via extracellular field potential and impedance. Impedance has been used in the past as an indirect measure of contractility. The medium was changed at least once in each 24-h period. Solutions were prepared in medium containing 15% FBS on the day of the experiment and kept at 37 °C until use. Wells were dosed under sterile conditions by removing 50% of the medium and replacing it by the same volume of fresh culture medium. The sensor plates were returned to the incubator immediately after dosing. Data were recorded continuously.

2.12. Echocardiography

Transthoracic echocardiograms were recorded in conscious, sedated mice with a Vevo 770 Imager (Visual Sonics). Briefly, mice were anesthetized with isoflurane. Fur was shaved from the upper sternal to subxiphoid areas. These areas were then moistened with the ultrasonic coupling agent. 2D images were acquired in left ventricle (LV); LV internal diameters and wall thicknesses were measured (at least three cardiac cycles) at end systole and end diastole. LV mass, volumes, and ejection fractions were calculated with the area-length method.

2.13. In vivo *over-expression of SORBS2 in wild-type C57 mice*

AAV9 vectors used for SORBS2 over-expression were from JIKAI Biotechnology. The recombinant AAV9 virus carrying SORBS2 cDNA with a cardiac-specific promoter CTNT (AAV-Ctnt-SORBS2-3flag) was used. 8-week-old mice were used for the AAV virus injection through jugular vein at a dose of 1.3 × 1013 vg per kg body weight. 10 wild-type C57 mice received AAV9-cTNT- SORBS2-3flag vector injections, and the wild-type mice (n = 10), in the control group, received AAV9-Ctnt-3flag injections at the same dose. After 3 weeks, these mice were evaluated via echocardiography. Heart tissues were collected after basic cardiac function was assessed. The transfection efficiency was assayed by fluorescence immunostaining. The results showed AAV virus transfection efficiency is at 53.45±3.76 (n = 4 hearts, each heart has 5 slides; representative image was shown in Fig. S6a).

2.14. Statistical analysis

All data were analyzed with SPSS 22. One-way analysis of variance (ANOVA) was used to assess differences between groups. In all analyses, P-values<0.05 and P-values<0.01 were considered indicative of a statistically significant difference.

3. Results

3.1. SORBS2 is specifically elevated in LVNC heart tissues, but not in HCM or ARVC

We initially conducted a proteomics analysis seeking to identify proteins differentially accumulated in heart tissues of patients with Left Ventricular Noncompaction Cardiomyopathy (LVNC; 8 samples), Hypertrophic Cardiomyopathy (HCM; 7 samples), and Arrhythmogenic Right Ventricular Cardiomyopathy (ARVC; 8 samples) (Fig. 1a). Our comparative analysis of the four sample types identified which proteins were significantly up-regulated (fold change>1.2) and down-regulated (fold change<0.83) in LVNC, HCM, and ARVC hearts, we present a Venn diagram depicting the overlaps amongst these sets of differentially accumulated proteins (Fig. 1b and c). We prepared a volcano chart to illustrate the comparisons between the LVNC, HCM, and ARVC groups with the normal control (NC) group (Fig. 1d−f).

Specifically, our proteomics analysis identified 45 proteins with significantly elevated expression in LVNC hearts (Table S2) that were not elevated in ARVC or HCM hearts. LVNC is characterized by an excessive trabecular meshwork of deep intertrabecular recesses

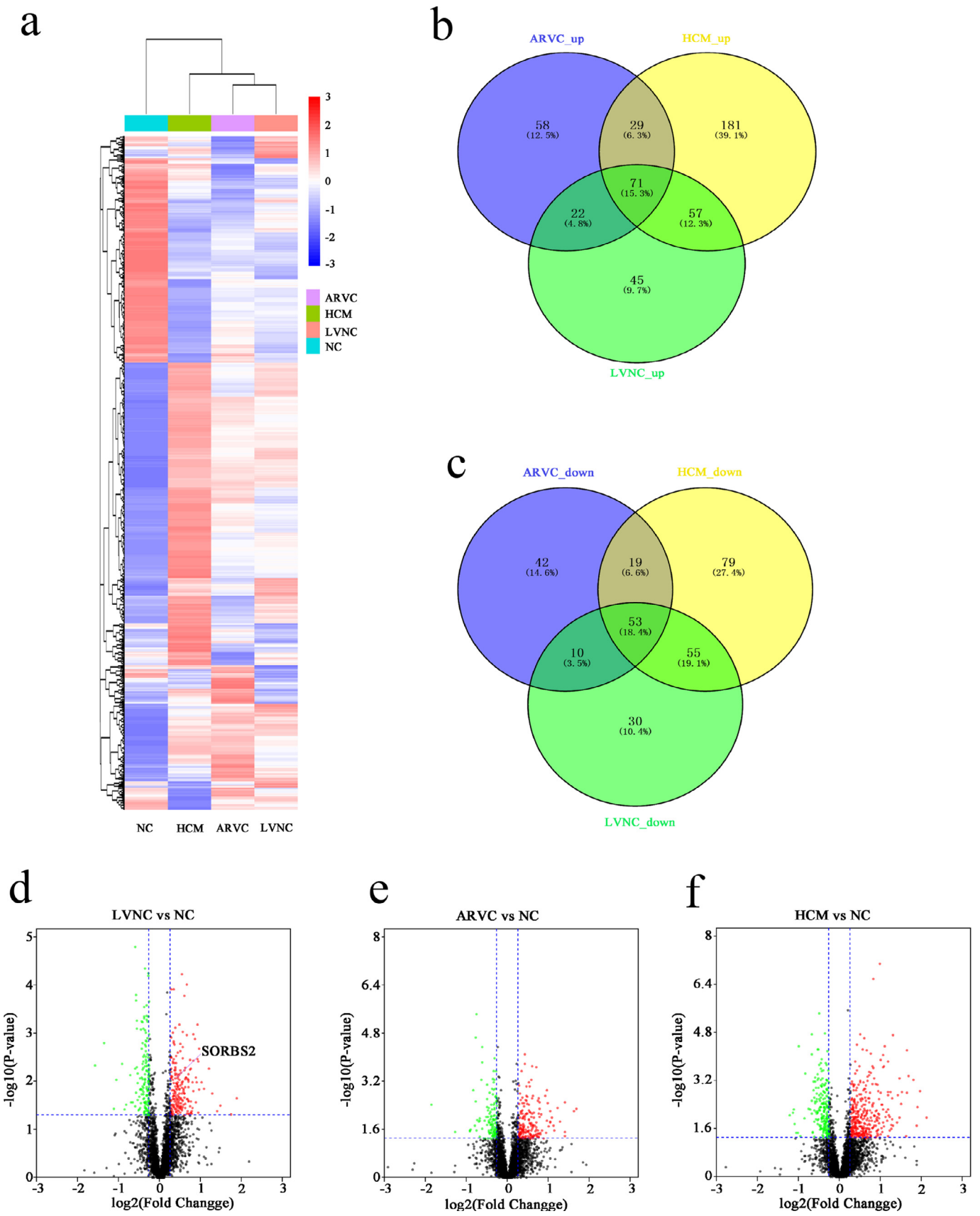

Fig. 1. Proteomics analysis of human cardiac tissues from ARVC, HCM, LVNC, and NC individuals. (a) Heatmap illustrating differentially accumulated proteins from the four groups of hearts obtained in the course of transplant surgeries. (b) and (c) Venn diagram indicating the numbers of differentially accumulated proteins (up and down) in the ARVC, HCM, and LVNC hearts. (d), (e) and (f) Volcano plots show the differentially expressed proteins among the four groups including ARVC, HCM, LVNC and NC. Green dots represent proteins whose expression was significantly decreased in cardiac tissues. Red dots represent proteins whose expression was significantly increased in cardiac tissues. Black dots represent proteins whose expression did not reach statistical significance. (For interpretation of the references to color in this figure legend, the reader is referred to the web version of this article.)

within the ventricular myocardium [27], which has been associated with the development and regulation of the cytoskeleton in heart tissue [28]. We analyzed 45 proteins in detail and found that the expression of SORBS2, which is mainly expressed in heart tissue and regulates cytoskeleton dynamics, is increased in LVNC, but not in ARVC or HCM. To validate the proteomics result for SORBS2, we performed western blotting of the heart tissues of the four groups. Consistent with the initial observation, we found that there was no difference from NC in SORBS2 accumulation in the HCM or ARVC hearts but that there was a significant increase in the SORBS2 level in the left ventricular myocardial tissues of patients with LVNC (Fig. 2a and b). Quantitative analysis of the immunoblotting signal revealed that the observed LVNC-specific increase in SORBS2 was statistically significant.

To explore this LVNC-specific regulated accumulation of SORBS2 in greater detail, we conducted immunohistochemistry analysis of prepared sections from the aforementioned human transplant materials. Specifically, SORBS2 was neatly distributed on the intercalated discs and Z-lines of normal control myocardium, but its distribution was disorganized on the intercalated discs and Z-lines of the LVNC tissues (Fig. 2c).

3.2. LVNC human heart tissues exhibit increased β-tubulin polymerization

Previous studies have shown that over expression of SORBS2 affects cytoskeleton rearrangements via regulation of β-tubulin polymerization [4]. We hypothesized that β-tubulin dynamic alteration may be subject to SORBS2 upregulation in LVNC. Using our prepared sections from heart transplant patients, immunofluorescence staining with an antibody against β-tubulin indicated that the LVNC hearts possessed increased β-tubulin density as compared to NC samples, suggesting microtubule hyper-densification in LVNC (Fig. 3a). We next used immunoblotting of tissue extracts to quantify both free and polymerized β-tubulin in the heart tissues. There was a significant increase in the formation of microtubule (including the level of polymerized β-tubulin (Fig. 3b and c) and a-tubulin (Fig. S2a and b)) in the left ventricular myocardial tissues of patients with LVNC.

3.3. SORBS2 interacts with β-tubulin and results in microtubule densification

To investigate whether the observed elevation in SORBS2 levels may promote β-tubulin polymerization, we conducted further immunofluorescence analysis and co-immunoprecipitation of SORBS2 and β-tubulin in normal hearts, which respectively revealed colocalization and interaction relationships between SORBS2 and β-tubulin in normal control hearts by immunofluorescence analyses and co-immunoprecipitation assays, respectively (Fig. 3d and e). Additionally, western blotting and immunostaining showed that 293T cells transfected with a lentivirus to overexpress SORBS2 (SORBS2-OE) exhibited aggravated microtubule polymerization as compared with control cells transfected with the empty vector control group (Fig. 3f–i). Taken together, these results support that the SORBS2 protein interacts with β-tubulin and facilitates polymerization of microtubules.

3.4. SORBS2 overexpression (SORBS2-OE) results in microtubule polymerization, junctophilin 2 (JP2) redistribution, and decreased mechanical activity in human embryonic stem cell derived cardiomyocytes (hESC CMs)

Previous studied have established that microtubule polymerization mediated by JP2 redistribution results in myocyte T-Tubule remodeling and Ca^{2+} handling dysfunctions that contribute to progressive heart failure [14]. Our present study detected an irregular and disordered distribution of JP2 in LVNC human hearts, although there was no obvious alteration of its expression level (Fig. 4a–c). We conducted experiments examining cardiomyocyte microtubule physiology in human embryonic stem cell (hESC) (Fig. S3a and b) derived cardiomyocytes (hESC CMs) (Fig. S3c). After assessing cell quality and successful differentiation into hESC CMs, we transfected these cells with an HBLV-h-SORBS2 lentivirus, which led to the successful overexpression of the SORBS2 protein (Fig. S3d–g). We used antibodies against both SORBS2 and β-tubulin for immunofluorescence analysis of these normal hESC CMs, which revealed obvious co-localization of these two proteins, thereby confirming the results from our analysis of the normal heart sections (Fig. 4d). These experiments also revealed that SORBS2 overexpression causes microtubule densification. Specifically, immunofluorescence staining showed that hESC CMs overexpressing SORBS2 had obviously higher levels of β-tubulin than empty-virus control cells (Fig. 4e and f), and immunoblotting analysis showed that SORBS2 overexpression increases the proportion of polymerized *versus* free β-tubulin (Fig. 4g and h).

We also observed that the hESC CMs overexpressing with SORBS2 had disorganized intracellular localization of JP2. In immunofluorescence experiments using antibodies against JP2 and its well-characterized interacting partner type two ryanodine receptor (RyR2), it was clear that the JP2 protein strongly overlaps with RyR2 in the empty vector control hESC-CMs; however, JP2 was uncoupled with RyR2 in hESC CMs overexpressing SORBS2 (Fig. 4i).

Excitation-contraction coupling (E-C coupling) function and Ca^{2+} handling of cardiomyocytes are both known to depend on JP2 and RyR2 pairing to some extent [14,17]. We therefore used the CardioExcyte 96 system to conduct impedance measurements of the contractions of the hESC-derived CMs. Both empty vector control and SORBS2-overexpressing hESC CMs were cultured in gelatin-coated 96 well impedance plates. We investigated the beating characteristics by pacing the two groups. The impedance measurements of the contractions of the hESC CMs were recorded, which revealed a decline in the amplitude of beating in the SORBS2-overexpressing hESC CMs as compared with the control group (Fig. 5a). Also, we found out SORBS2 overexpressing hESC CMs decreased cardiomyocyte mechanical activity over the same time period as the calcium recordings, compared with control group (Fig. 5b) in the one single cell. Thus, SORBS2 overexpression markedly weakens the mechanical activity of hESC-derived cardiomyocytes.

3.5. Cardiac specific overexpression of SORBS2 manifested cardiac dysfunction, β-tubulin aggregation, and JP2 translocation in vivo

Our results from the heart-transplant LVNC tissue samples and our hESC CMs experiments showed that SORBS2 enhances β-tubulin polymerization, JP2 translocation and cardiomyocytes dysfunction. Next, we tested the potential mechanism through which SORBS2 contributes to disruption of mechanical cardiac function *in vivo* by conducting studies in mice which sought to further extend our understanding of how SORBS2 may drive the heart failure progression or development of LVNC. We used adeno-associated virus (AAV9) to over express SORBS2 in the cardiac left ventricle tissues of wild-type mice, and subsequently assessed various cardiac phenotypes. The experimental flowchart was as follows (Fig. 6a). Confirming the expression and location of SORBS2, the expression of SORBS2 in the mice injected with the AAV9-cTNT-SORBS2-3flag virus was increased compared to empty-virus control mice (Fig. 6b and c). Immunocytochemistry and immunofluorescence results both showed that SORBS2 was localized in the Z-bands of mouse cardiac tissues (Fig. 6d–g).

Furthermore, we measured several echocardiographic parameters before the virus (AAV9) was injected and assessed the ejection fraction (EF) (Fig. S4a). After three weeks, we measured the echocardiographic analysis of the mice revealed obvious differences in cardiac

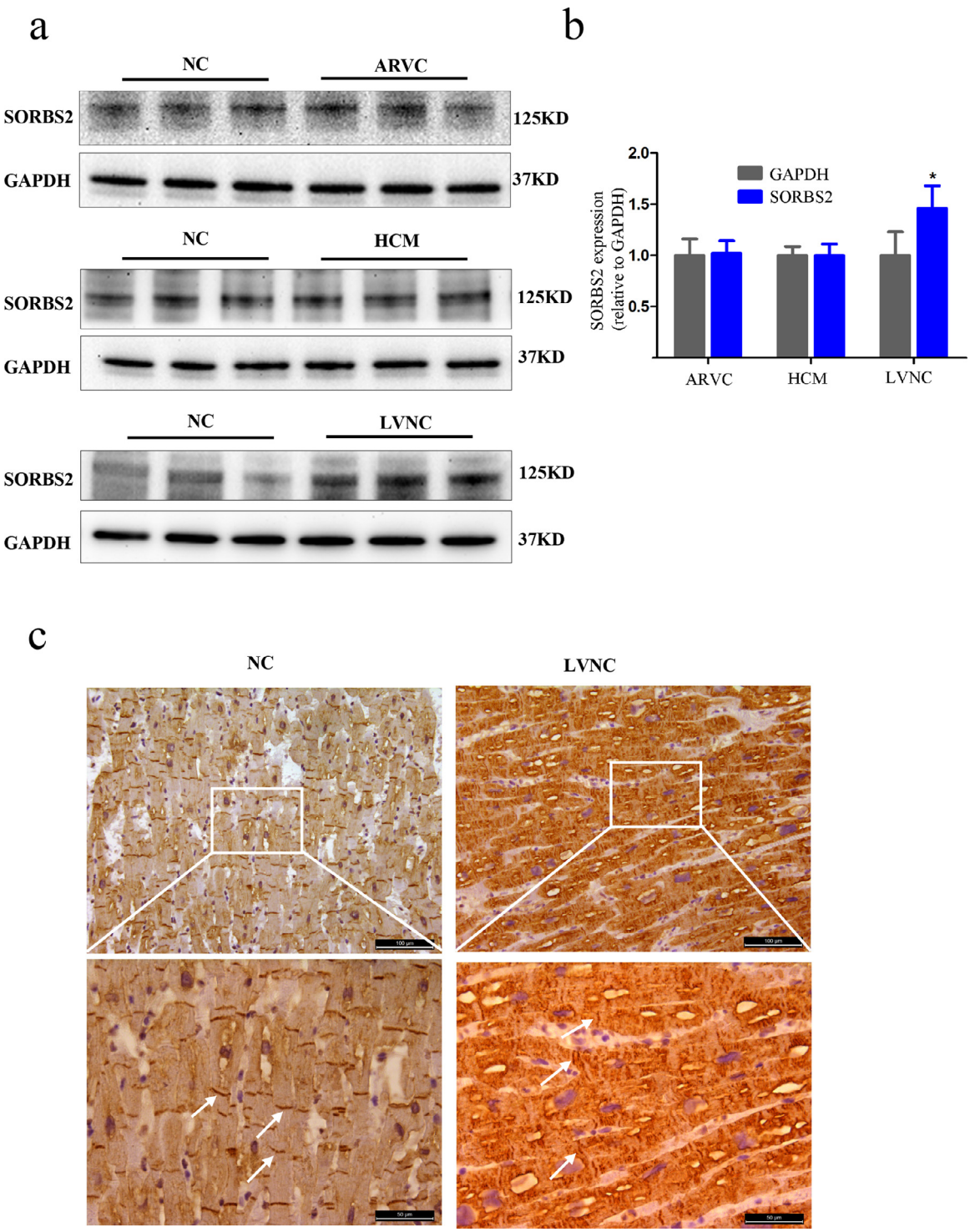

Fig. 2. Expression and localization of SORBS2 in human cardiac tissues. (a) Western blot analysis showing protein levels of SORBS2 in human hearts obtained from transplant patients diagnosed with ARVC, HCM, or LVNC. (b) Statistical analysis of the SORBS2 protein levels in ARVC, HCM, LVNC and healthy control hearts. (n = 5 for each group, * $p < 0.05$). Data are shown as mean ± SEM; a Student's t-test was used for inferential statistical analysis. (c) Representative images of the distribution of SORBS2 protein in LVNC and normal human hearts assessed using immunohistochemistry. White arrows represent SORBS2 localized in the Z-bands. The white box in the upper panels represents the areas enlarged in the lower panels; scale bars represent 100 μm in the upper panel and 50 μm in the lower panel. n = 3 for each group.

function: the SORBS2 overexpression mice had significantly reduced ejection fractions (38%) compared to the control group (58%, $p < 0.01$) (Fig. 6h–j), other relevant indicators were shown in Fig. S4b–e.

Next, immunofluorescence staining and western blotting of the cardiac left ventricle tissues with enhanced expression of SORBS2 revealed microtubule hyper-densification and JP2 redistribution (Fig. 7a–c). And we also observed interaction relationship between SORBS2 and β-tubulin in control mice tissues (Fig. S5a). Altering the JP2 distribution within the membrane system is known to contribute to defective E-C coupling in heart failure, which is reflected by T-tubule remodeling and Ca^{2+} cycling dysfunction [18]. We conducted immunofluorescence staining against the flag tag of the over-expression SORBS2 protein, and found that the transfection efficiency of AAV9-injected mice was 53.45 ± 3.76% (Fig. S6a). We

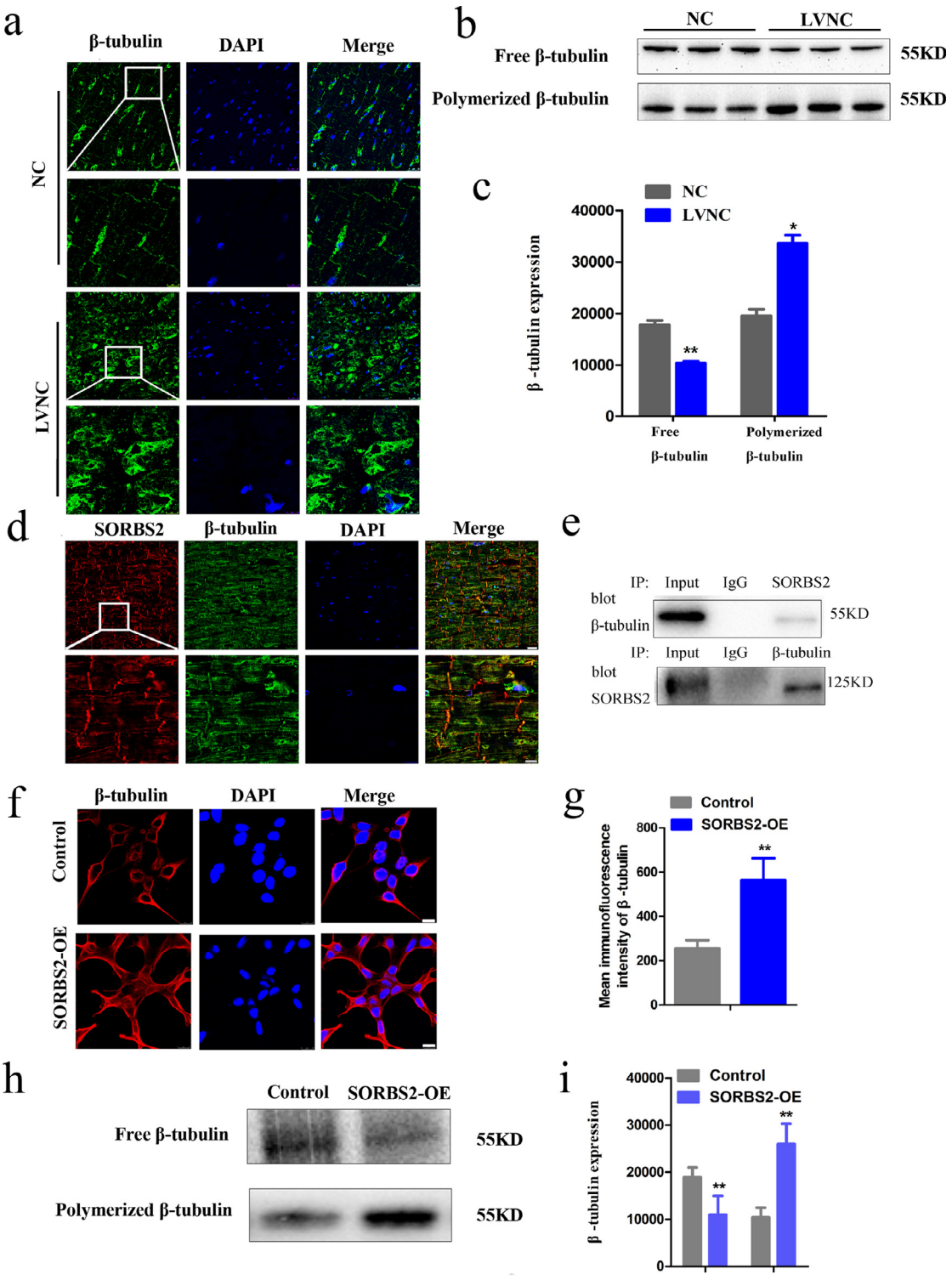

Fig. 3. Microtubule densification in LVNC myocardial tissues and in 293T cells with HBLV-h-SORBS2 lentivirus transfection. (a) Highly expressed β-tubulin in LVNC hearts compared to normal control hearts by immunofluorescence analyses. The white box in the upper panels indicates the areas enlarged in the lower panels; (scale bars: 25 μm, 10 μm). (b) and (c) The decreased level of free β-tubulin and the increased level of polymerized β-tubulin in LVNC hearts compared to normal control hearts by western blotting analyses. (n = 4 for normal hearts and n = 5 for LVNC hearts, $^{*}p < 0.05$, $^{**}p < 0.01$). Data shown as mean ± SEM; a Student's t-test was used for the inferential statistical analysis. (d) Co-localization of SORBS2 (red) and β-tubulin (green) in human cardiac tissues. The co-localized SORBS2 and β-tubulin proteins are visualized in yellow in these human cardiac tissues. The white box in the upper panels represent the areas enlarged in the lower panels (scale bars: 25 μm, 10 μm). (e) An interaction relationship between SORBS2 and β-tubulin in normal control hearts by Co-immunoprecipitation assays. Extracted proteins from all the above mentioned tissues were untreated (input) and the rabbit (IgG) were set as positive and negative controls respectively. SORBS2 antibodies were used for Co-immunoprecipitation (Co-IP), β-tubulin antibody was used or western blot. Likewise, β-tubulin antibodies were used for Co-IP, SORBS2 antibody was used for western blot. Co-immunoprecipitation (Co-IP) of the tissues showing SORBS2 binding with β-tubulin. (f) and (g) Representative images of β-tubulin immunofluorescence staining of 239T cells transfected with HBLV-h-SORBS2 and empty-virus control cells. The expression of β-tubulin in control was decreased compared to the SORBS2 overexpression 293T cells. (n = 25−30 cells per group, $^{**}p < 0.01$; Student's t-test) (h) and (i) Immunoblotting to assess the β-tubulin level of 239T cells. Quantitative analysis of the expression of β-tubulin in both its free (F) and polymerized (P) forms (n = 3 per group, $^{**}p < 0.01$; Student's t-test). SORBS2-OE: 293T cells transfected with HBLV-h-3*flag-GFP-SORBS2 lentivirus. Control: 293T cells transfected with HBLV-GFP-PURO-NC lentivirus. (For interpretation of the references to color in this figure legend, the reader is referred to the web version of this article.)

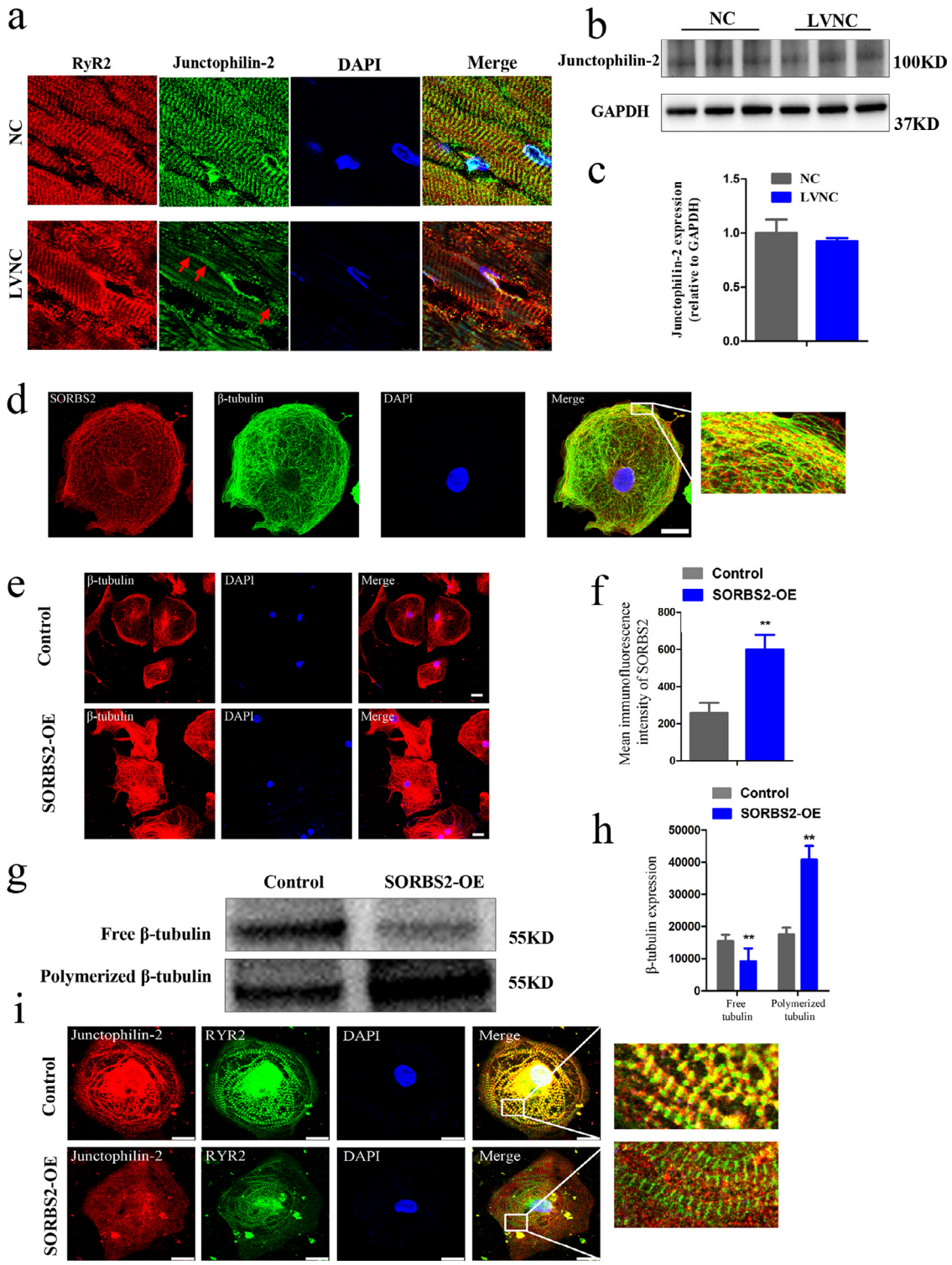

Fig. 4. Characterization of β-tubulin and JP2 localization and functions in hESC-derived cardiomyocytes overexpressing SORBS2. (a)Representative confocal images of JP2 immunofluorescence staining of LVNC and control heart sections. (scale bars: 10 μm). (b) and (c) Representative immunoblot for the JP2 level in LVNC and control hearts. Quantitative analysis of the JP2 protein level in the LVNC and control hearts (n = 4 for normal hearts and n = 5 for LVNC hearts). Data shown as mean ± SEM; a Student's t-test was used for the inferential statistical analysis. (d) Co-localization of SORBS2 and β-tubulin in hESC-derived cardiomyocytes. Immunohistochemical staining of SORBS2 (red) and β-tubulin (green) proteins; the co-localized SORBS2 and β-tubulin proteins are visualized in yellow in these in hESC-derived cardiomyocytes. Nuclei were stained with DAPI (blue) The white box in the left panels represents the areas enlarged in the right panels (scale bars: 25 μm). (e) and (f) Representative images of β-tubulin immunofluorescence staining of hESC-derived CMs transfected with HBLV-h-SORBS2 and empty-virus control cells. Quantitative analysis of the expression of β-tubulin in control and SORBS2 overexpression hESC-CMs. (n = 25–30 cells per group, $^{**}p < 0.01$; Student's t-test). (g) and (h) Immunoblotting to assess the β-tubulin level of hESC-derived cardiomyocytes. Quantitative analysis of the expression of β-tubulin in both its free (F) and polymerized (P) forms. Data shown as mean ± SEM; a Student's t-test was used for the inferential statistical analysis. (i) Representative images of immunofluorescence signals for JP2 and RyR2 in hESC-derived CMs. The white box in the left panels represents the areas enlarged in the right panels (scale bars: 25 μm). SORBS2-OE: hESC-CMs transfected with HBLV-h-3*flag-GFP-SORBS2 lentivirus. Control: hESC-CMs transfected with HBLV-GFP-PURO-NC lentivirus. (For interpretation of the references to color in this figure legend, the reader is referred to the web version of this article.)

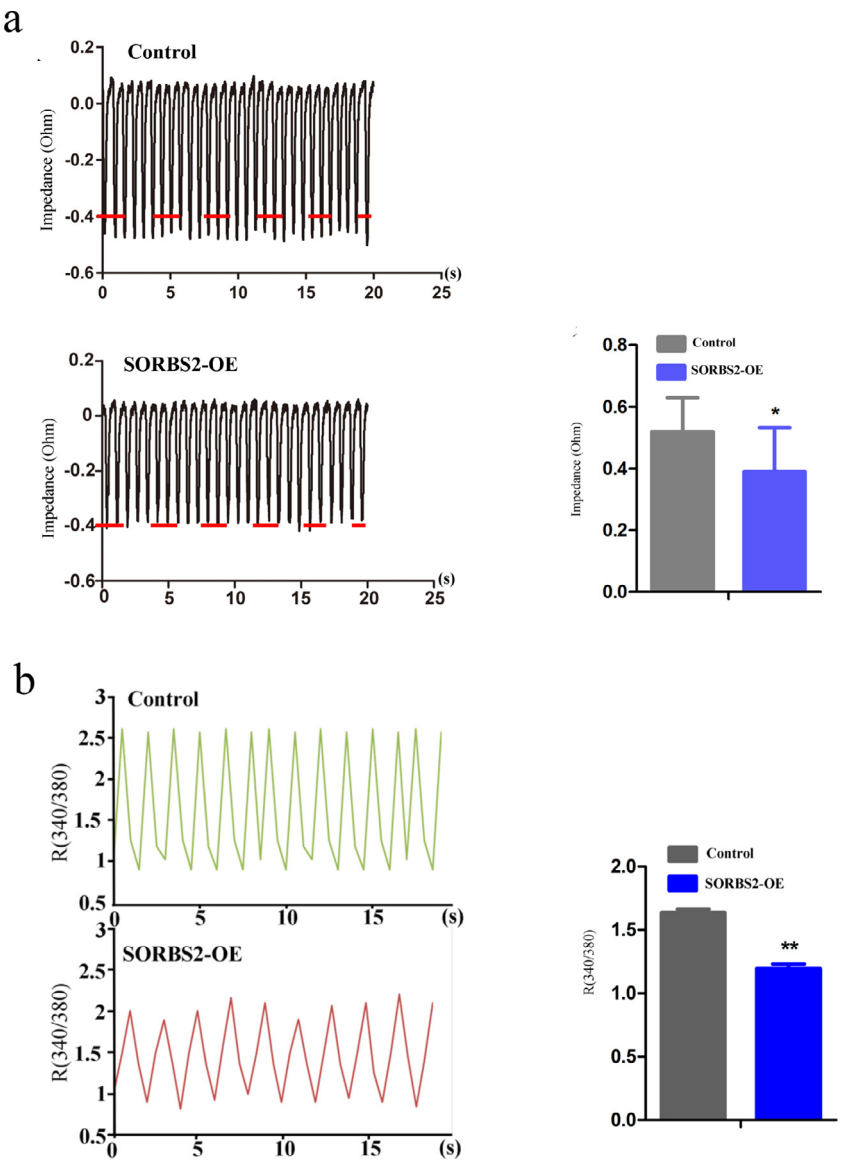

Fig. 5. Effects of SORBS2 overexpression on contraction function of cardiomyocytes. (a) Raw traces of impedance detected by CardioExcyte 96 system in SORBS2-OE and control group. The decreased impedance signal was observed in SORBS2-OE group ($n = 3$ for each group, $^{*}p < 0.05$; Student's *t*-test). Data shown as the mean ± SEM. (b) Raw traces of intracellular calcium transients detected by calcium imaging in SORBS2-OE and control group. The decrease in the intracellular calcium transients was found in SORBS2-OE group ($n = 8$ cells per group, $^{**}p < 0.01$; Student's *t*-test). Data shown as the mean ± SEM.

performed T-tubule imaging on control and SORBS2 over-expression groups. As compared with the control group, over-expression of SORBS2 represented unordered T-tubule network (Fig. 7d). We performed Ca^{2+} imaging on isolated cardiomyocytes from the control and SORBS2 over expression groups. As compared with the control group, over expression of SORBS2 represented depressed Ca^{2+} amplitude and prolonged time to reach peak (Fig. 7e–g). Also, evaluation of time to calcium decay 50% is also valid since it looks much longer in the AAV9-SORBS2-transduced mice (Fig. 7h). Later, we conducted co-immunoprecipitation of SORBS2 and JP2, co-immunoprecipitation of SORBS2 and RyR2 in normal human heart tissues, there were no interactions relationship between SORBS2 and JP2, the same effect showed in the SORBS2 and RyR2 (Fig. S2c). And also, the expression of RyR2 had no change both in LVNC human hearts and in SORBS2 over expressing hESC-derived CMs (Fig. S2d–g). All data demonstrated that over expression of SORBS2 could mediate β-tubulin aggregation, JP2 translocation and E-C coupling dysfunction *in vivo*.

4. Discussion

Left ventricular noncompaction cardiomyopathy (LVNC) is associated with left ventricular diastolic and systolic dysfunction. The myocardial wall is often thickened with a thin, compacted epicardial layer and a thickened endocardial layer. One of LVNC guidelines is to prevent the progression and development of heart failure [29].

LVNC has gained increasing attention in recent years [30] because of its association with high rates of mortality and morbidity in adults, including heart failure, arrhythmias, and thromboembolic events [31–33]. LVNC may be due to the arrest of the normal compaction process of the myocardial wall during fetal development [34]. Numerous genetic disorders have been reported to be associated with LVNC, including sarcomere and Z-disk gene mutations [35,36]. Regardless of the complicated heterogenous causes of LVNC [37], heart failure is one of the most common clinical consequences in LVNC patients, but the relationship between LVNC and heart failure is not well understood and requires further study [35,36]. All the

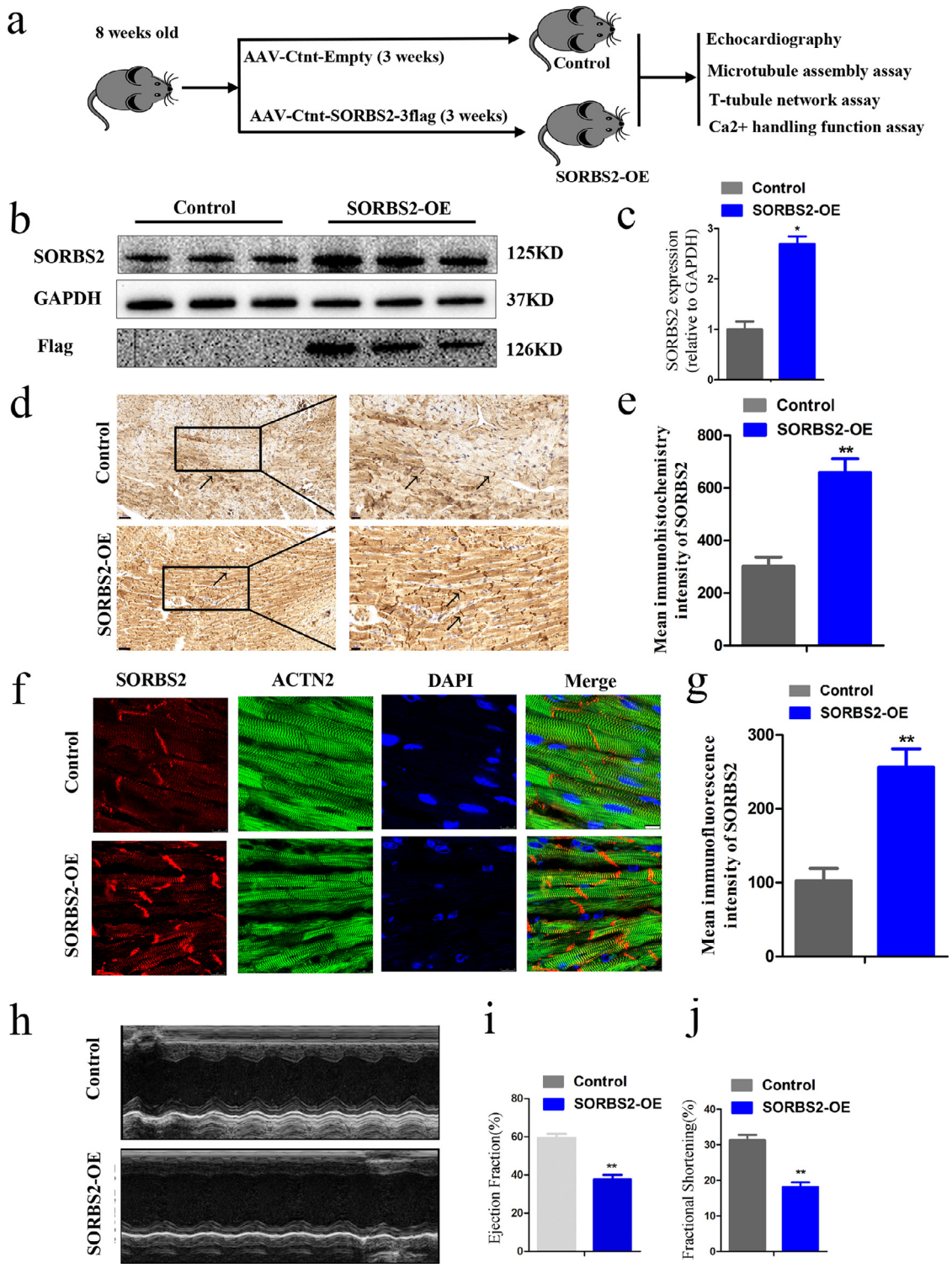

Fig. 6. Establishment and verification of transgenic mice overexpressing SORBS2 *in vivo*. (a) flowchart *in vivo*. (b) and (c) Immunoblotting was used to assess the accumulation of the SORBS2 protein in cardiac tissues from harvested mice injected with control or SORBS2 overexpression AAV9 vectors. ($n = 5$ for each group, * $p < 0.05$; Student's *t*-test). Data shown as the mean ± SEM. (d) and (e) SORBS2 protein accumulation analyzed by immunohistochemistry staining; Black arrows represent SORBS2 localized in the Z-bands. The black box in the left panels indicates the areas enlarged in the right panels (scale bars represent 50 μm, 20 μm, respectively). Statistical analysis of the SORBS2 quantitative analysis levels in mice tissues. ($n = 5$ for each group, ** $p < 0.01$; Student's *t*-test). Data shown as the mean ± SEM. (f) and (g) Representative images of SORBS2 immunofluorescence staining of mice tissues (scale bars: 25 μm). Statistical analysis of the SORBS2 quantitative analysis levels in mice tissues. ($n = 5$ for each group, ** $p < 0.01$; Student's *t*-test). Data shown as the mean ± SEM. (h) Representative short-axis M-mode images of hearts from control and SORBS2 overexpression mice. (i) and (j) Ejection Fraction (EF) and Fractional Shortening (FS) of the control and SORBS2 overexpression mice were detected by Echocardiographic assessment. ($n = 5$ for each group, ** $p < 0.01$; Student's *t*-test). Data shown as the mean ± SEM. SORBS2-OE: experiment group (the wild-type C57 mice received AAV9-cTNT-SORBS2-3flag vector injections through jugular vein), Control: control group (the wild-type C57 mice received AAV9-cTNT-3flag vector injections through jugular veins).

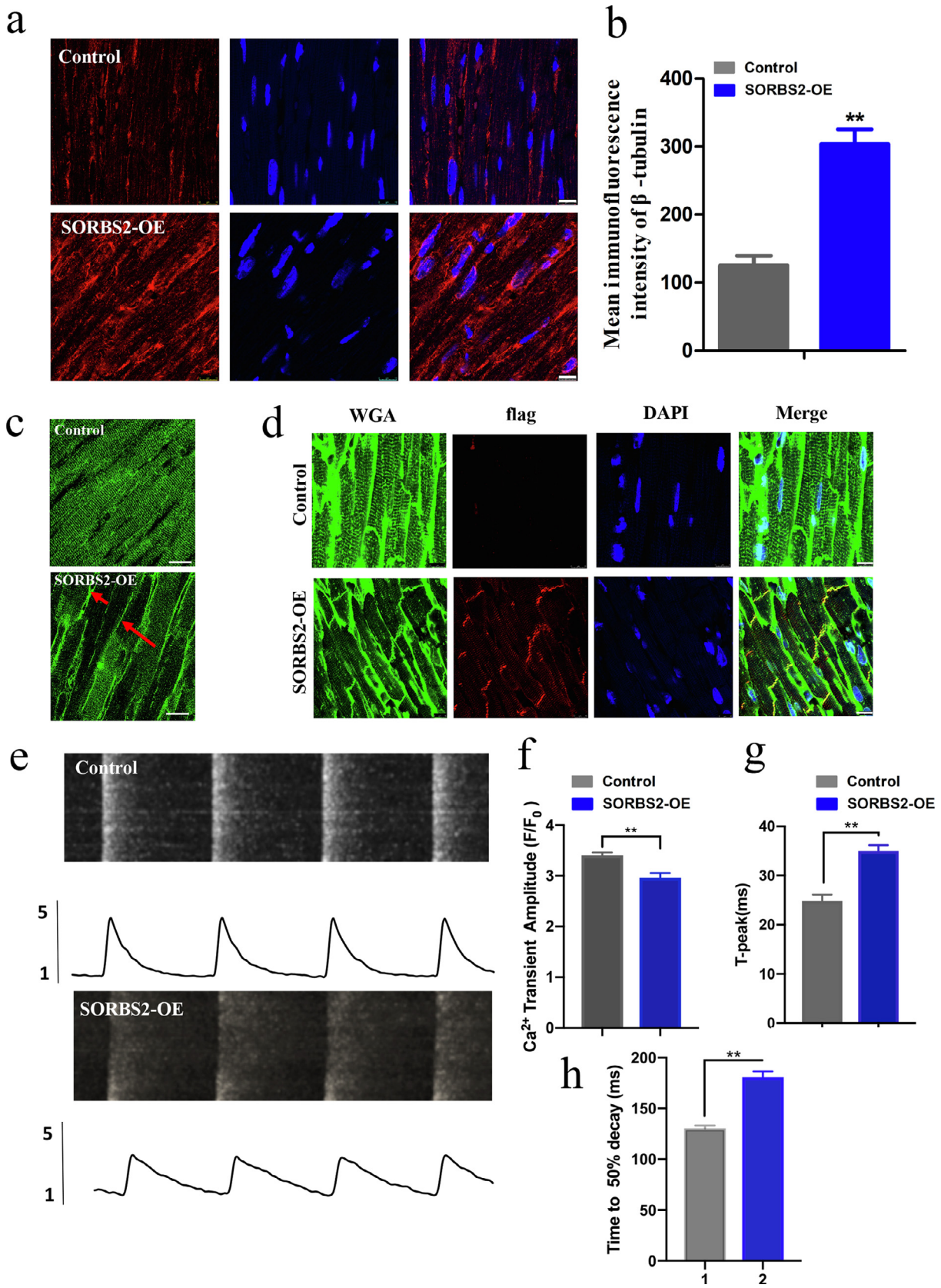

Fig. 7. Effects of *in vivo* overexpressed SORBS2 on cardiac structure and function in mice. (a) and (b) Immunofluorescence staining against β-tubulin (scale bars: 10 μm). Statistical analysis of the β-tubulin quantitative analysis levels in mice tissues. (n = 5 for each group, ** $p < 0.01$; Student's t-test). Data shown as the mean ± SEM. (c) Representative images of JP2 immunofluorescence staining of mice tissues. Red arrows mean that JP2 moved to merge in cardiac tissues from harvested mice injected with SORBS2 overexpression AAV9 vectors. (d) Immunofluorescence staining against T-tubule with WGA in mice tissues. (scale bars: 10 μm). (e) Representative cytosolic Ca^{2+} images (upper) and traces (lower) in freshly isolated cardiomyocytes from hearts transfected with empty virus and SORBS2 overexpression virus. (f) and (g) Average data of the amplitude and time to peak of Ca^{2+} transients. (n = 6–10 cells from one heart, n = 5 each group). (h) The statistical analysis of evaluation of time to calcium decay 50%.

8 LVNC patients waiting for heart transplantation, used in our proteomic analyses, suffered from heart failure with severely reduced LV ejection fraction (EF) of 18%−37%. In this study, our primary intention is focused on the identification of the key signaling pathway whose dysfunction has a causal role in the occurrence of heart failure in LVNC patients, but not on the molecular mechanism of LVNC.

The left ventricle (LV) heart samples used in our study were obtained from heart transplantation patients clinically diagnosed with LVNC on the basis of echocardiographic or CMR documentation, and autopsy findings of explanted hearts, with a distinct two-layered appearance of trabeculated and compacted myocardium. Using comparative proteomic analyses, we identified 45 proteins up-regulated in LVNC hearts but not in HCM and ARVC hearts. SORBS2, one of the up-regulated proteins that have not been reported previously in LVNC, attracted our interest because SORBS2 is a sarcomere protein at the Z-band and intercalated disk [38], and mutations in genes encoding sarcomere proteins have been reported to be a risk factor for heart failure in LVNC [38]. Prior to our findings, no data was available regarding the role of SORBS2 in LVNC. Previous studies reported that SORBS2 acts as a sarcomeric protein that functions in cell adhesion, cytoskeletal organization, and signal transduction pathways by recruiting various molecules to critical areas in cells [39], and levels of SORBS2 are much higher in the heart than those in the other tissues [40]. In this study, whether and how SORBS2 is involved in the pathogenesis of heart failure in LVNC is our big concern.

This study aims to investigate whether a novel molecular mechanism contributes to heart failure progression in LVNC by performing *in vitro* and *in vivo* studies. The major study conclusions are as follows: (I) SORBS2 is a protein specifically upregulated in LVNC, but not in HCM and ARVC groups; (II) Densification of microtubules was shown in LVNC human cardiac tissues as well as in hESC-derived cardiomyocytes over expressing SORBS2 and heart tissue from the mice over expressing SORBS2; (III) SORBS2 co-immunoprecipitated with β-tubulin in myocardium and boosted β-tubulin densification; (IV) SORBS2 over expression can result in microtubule-mediated Junctophilin 2 (JP2) distribution tubulin in hESC-derived cardiomyocytes and the myocardial tissues; (V) Mice displaying SORBS2 over expression presented cardiac failure, followed by tubulin polymerization, T-tubule damage and Ca^{2+} cycling procession damage. Taken together, our study provides unique insights into the upregulated SORBS2-induced β-tubulin densification, so as to affect the redistribution of JP2 and T-tubule disorganization, contributing to the cardiac failure in the LVNC.

Previous studies [41] have identified patients diagnosed with LVNC carry potentially pathogenic mutations in genes including TPM1, TNNC1, and ACTC1. Human-induced pluripotent stem cells (hiPSCs) from a patient carrying a TPM1 p.Arg178 His mutation who underwent heart transplantation displayed disruption of the sarcomere structure in cardiomyocytes, as well as impaired calcium handling. Our findings in the present study suggest similar disruption is associated with SORBS2: we show that SORBS2 promotes the densification of microtubule-mediated Ca^{2+} handling disorder and heart failure by promoting microtubule densification, driving Ca^{2+} handling dysfunction, and altering the distribution of JP2 and the T-tubule network.

SORBS2 is a protein widely expressed in human tissues, such as heart, brain, spleen, pancreas, and kidney. In epithelial cells, SORBS2 is located in stress fibers [40]. Silencing of SORBS2 reverted the tubulogenesis and SORBS2 is a key effector of Bα-mediated regulation of cytoskeletal rearrangements in ECs [4]. In heart tissues with ischemia disease, SORBS2 is dramatically reduced in infarcted myocardia [3]. In addition, SORBS2 has no any alteration in the HCM and ARVC, as compare to normal control (NC) group. Interestingly, in our study, SORBS2 is highly expressed in LVNC. All these data give us a clue that SORBS2 upregulation maybe a unique phenomenon among heart disease. Further, we determined that SORBS2 is highly associated with the progress of heart failure in the LVNC disease, as SORBS2 over expression, can aggravate microtubule density and β-tubulin polymerization *in vivo* or *in vitro*, and eventually exacerbate cardiac dysfunction. Therefore, SORBS2 upregulation mediated β-tubulin polymerization and excitation-contraction coupling (E-C coupling) dysfunction may facilitate heart failure in LVNC.

Microtubule densification due to increased expression of tubulin and formation of stable microtubules have been observed in multiple models at the compensated and decompensated stages of myocardial hypertrophy [11,42,43]. Multiple mechanisms have been proposed to explain how the densification of the microtubule network can lead to cardiac dysfunction. One such mechanism is that microtubule densification somehow alters JP2 distribution, E-C coupling, T-tubule network and Ca^{2+} handling disorder, which gives rise to impairment of cardiomyocytes contraction. Zhang et al. showed altered JP2 localization from the middle membrane to the surface plasma membrane in response to stresses that induce microtubule densification. Their study identified the translocation of JP2 as a cause of T-tubule remodeling in heart disease and in cultured adult cardiomyocytes [14]. We detected JP2 redistribution in LVNC human heart tissues, hESC-derived cardiomyocytes and mouse heart tissue with SORBS2 over expression. Furthermore, over expression of SORBS2 *in vivo* leads to T-tubule disorganization and Ca^{2+} handling dysfunction. All these data demonstrated a novel pathway involving SORBS2 over expression β-tubulin densification JP2 translocation and therefore T-tubule disorganization is implicated in the development and progression of heart failure in LVNC disease.

Several limitations should be considered in the present study. First, because our experiments are confined to adult mice subjected to virus-mediated SORBS2 over expression, future studies should focus on embryo or younger animals with enhanced over-expression of SORBS2 to determine whether they exhibit typical phenotypes of LVNC (*i.e.*, whether SORBS2 over expression in the embryo could produce the phenotype of excessive trabecular meshwork of deep intertrabecular recesses within the ventricular myocardium). Second, although SORBS2 interacts with microtubules and promotes their densification, the detailed mechanism by which SORBS2 aggravates microtubule formation still needs to be studied. Finally, due to lack of equipment to performed *in situ* heart T-tubule and Ca^{2+} imaging, we obtained the data of T-tubule network and Ca^{2+} handling from the isolated cardiomyocytes.

In summary, our proteomics-based analysis of tissues from transplant surgeries revealed that SORBS2 levels are significantly elevated in LVNC hearts but not in HCM or ARVC hearts. We confirmed that over-expression of SORBS2 in hESC-derived CMs (*in vitro*) and mice (*in vivo*) obviously increased microtubule formation, JP2 translocation, T-tubule network damage, and Ca^{2+} cycling disorder, collectively contributing to cardiomyocytes contraction dysfunction or heart failure (Fig. S7a). This study may have reference value for future development of targeting therapeutic strategies to postpone heart remodeling and the progression of heart failure in LVNC.

Declaration of competing interest

None.

Acknowledgments

Thanks for Ms. Qing Xu of Capital Medical University for the echocardiography.

Data Availability

The mass spectrometry data from the proteomics analysis has been deposited at Mendeley Data, a platform for sharing citable research datasets online, with the following ID: DOI: 10.17632/v3k385htnt.1

Funding Sources

This work was supported by the CAMS Initiative for Innovative Medicine (CAMS-I2M, 2016-I2M-1-015 to Y.J.Wei, who took part in the study design, data collection, data analysis and writing).

Supplementary materials

Supplementary material associated with this article can be found in the online version at doi:10.1016/j.ebiom.2020.102695.

References

[1] Arbustini E, Weidemann F, Hall JL. Left ventricular noncompaction: a distinct cardiomyopathy or a trait shared by different cardiac diseases? J Am Coll Cardiol 2014;64(17):1840–50.
[2] Kulhari A, Kalra N, Sila C. Noncompaction cardiomyopathy and stroke: case report and literature review. J Stroke Cerebrovasc Dis 2015;24(8):e213–7.
[3] Kakimoto Y, Ito S, Abiru H, Kotani H, Ozeki M, Tamaki K, et al. Sorbin and SH3 domain-containing protein 2 is released from infarcted heart in the very early phase: proteomic analysis of cardiac tissues from patients. J Am Heart Assoc 2013;2(6):e000565.
[4] Martin M, Geudens I, Bruyr J, Potente M, Bleuart A, Lebrun M, et al. PP2A regulatory subunit balpha controls endothelial contractility and vessel lumen integrity via regulation of HDAC7. EMBO J 2013;32(18):2491–503.
[5] Drew NK, Johnsen NE, Core JQ, Grosberg A. Multiscale characterization of engineered cardiac tissue architecture. J Biomech Eng 2016;138(11):111003–1–8.
[6] Baena-Lopez LA, Baonza A, Garcia-Bellido A. The orientation of cell divisions determines the shape of drosophila organs. Curr Biol 2005;15(18):1640–4.
[7] Preau S, Montaigne D, Modine T, Fayad G, Koussa M, Tardivel M, et al. Macrophage migration inhibitory factor induces contractile and mitochondria dysfunction by altering cytoskeleton network in the human heart. Crit Care Med 2013;41(7):e125–33.
[8] Zile MR, Green GR, Schuyler GT, Aurigemma GP, Miller DC, Gt Cooper. Cardiocyte cytoskeleton in patients with left ventricular pressure overload hypertrophy. J Am Coll Cardiol 2001;37(4):1080–4.
[9] Wang X, Li F, Campbell SE, Gerdes AM. Chronic pressure overload cardiac hypertrophy and failure in guinea pigs: II. Cytoskeletal remodeling. J Mol Cell Cardiol 1999;31(2):319–31.
[10] Tagawa H, Koide M, Sato H, Zile MR, Carabello BA, Gt Cooper. Cytoskeletal role in the transition from compensated to decompensated hypertrophy during adult canine left ventricular pressure overloading. Circ Res 1998;82(7):751–61.
[11] Takahashi M, Tsutsui H, Tagawa H, Igarashi-Saito K, Imanaka-Yoshida K, Takeshita A. Microtubules are involved in early hypertrophic responses of myocardium during pressure overload. Am J Physiol 1998;275(2):H341–8.
[12] Wang X, Gerdes AM. Chronic pressure overload cardiac hypertrophy and failure in guinea pigs: III. Intercalated disc remodeling. J Mol Cell Cardiol 1999;31(2):333–43.
[13] Prins KW, Asp ML, Zhang H, Wang W, Metzger JM. Microtubule-mediated misregulation of junctophilin-2 underlies T-Tubule disruptions and calcium mishandling in mdx mice. JACC Basic Transl Sci 2016;1(3):122–30.
[14] Zhang C, Chen B, Guo A, Zhu Y, Miller JD, Gao S, et al. Microtubule-mediated defects in junctophilin-2 trafficking contribute to myocyte transverse-tubule remodeling and Ca2+ handling dysfunction in heart failure. Circulation 2014;129(17):1742–50.
[15] Gomez AM, Kerfant BG, Vassort G. Microtubule disruption modulates Ca(2+) signaling in rat cardiac myocytes. Circ Res 2000;86(1):30–6.
[16] Calaghan SC, Le Guennec JY, White E. Modulation of Ca(2+) signaling by microtubule disruption in rat ventricular myocytes and its dependence on the ruptured patch-clamp configuration. Circ Res 2001;88(4):E32–7.
[17] Wang Y, Chen B, Huang CK, Guo A, Wu J, Zhang X, et al. Targeting calpain for heart failure therapy: implications from multiple murine models. JACC Basic Transl Sci 2018;3(4):503–17.
[18] Guo A, Wang Y, Chen B, Wang Y, Yuan J, Zhang L, et al. E-C coupling structural protein junctophilin-2 encodes a stress-adaptive transcription regulator. Science 2018;362(6421):eaan3303.
[19] Wasserstrom JA, Holt E, Sjaastad I, Lunde PK, Odegaard A, Sejersted OM. Altered E-C coupling in rat ventricular myocytes from failing hearts 6 wk after MI. Am J Physiol Heart Circ Physiol 2000;279(2):H798–807.
[20] Song LS, Sobie EA, McCulle S, Lederer WJ, Balke CW, Cheng H. Orphaned ryanodine receptors in the failing heart. Proc Natl Acad Sci U S A 2006;103(11):4305–10.
[21] Wu CY, Chen B, Jiang YP, Jia Z, Martin DW, Liu S, et al. Calpain-dependent cleavage of junctophilin-2 and T-tubule remodeling in a mouse model of reversible heart failure. J Am Heart Assoc 2014;3(3):e000527.
[22] Du H, Liu S, Li C, Wei Y. Comparative proteomics analysis of myocardium in left ventricular non-compaction cardiomyopathy. Acta Biochim Biophys Sin 2019;51(6):653–5.
[23] Tsutsui H, Ishihara K, Gt Cooper. Cytoskeletal role in the contractile dysfunction of hypertrophied myocardium. Science 1993;260(5108):682–7.
[24] Ostlund Jr. RE, Leung JT, Hajek SV. Biochemical determination of tubulin-microtubule equilibrium in cultured cells. Anal Biochem 1979;96(1):155–64.
[25] Qu L, Li Y, Pan X, Zhang P, LaMotte RH, Ma C. Transient receptor potential canonical 3 (TRPC3) is required for IgG immune complex-induced excitation of the rat dorsal root ganglion neurons. J Neurosci 2012;32(28):9554–62.
[26] Grynkiewicz G, Poenie M, Tsien RY. A new generation of Ca2+ indicators with greatly improved fluorescence properties. J Biol Chem 1985;260(6):3440–50.
[27] Garcia-Pavia P, de la Pompa JL. Left ventricular noncompaction: a genetic cardiomyopathy looking for diagnostic criteria. J Am Coll Cardiol 2014;64(19):1981–3.
[28] Ichida F. Left ventricular noncompaction - Risk stratification and genetic consideration. J Cardiol 2020;75(1):1–9.
[29] Gati S, Rajani R, Carr-White GS, Chambers JB. Adult left ventricular noncompaction: reappraisal of current diagnostic imaging modalities. JACC Cardiovasc Imaging 2014;7(12):1266–75.
[30] Maron BJ, Towbin JA, Thiene G, Antzelevitch C, Corrado D, Arnett D, et al. Contemporary definitions and classification of the cardiomyopathies: an American heart association scientific statement from the council on clinical cardiology, heart failure and transplantation committee; quality of care and outcomes research and functional genomics and translational biology interdisciplinary working groups; and council on epidemiology and prevention. Circulation 2006;113(14):1807–16.
[31] Ritter M, Oechslin E, Sutsch G, Attenhofer C, Schneider J, Jenni R. Isolated noncompaction of the myocardium in adults. Mayo Clin Proc 1997;72(1):26–31.
[32] Oechslin EN, Attenhofer Jost CH, Rojas JR, Kaufmann PA, Jenni R. Long-term follow-up of 34 adults with isolated left ventricular noncompaction: a distinct cardiomyopathy with poor prognosis. J Am Coll Cardiol 2000;36(2):493–500.
[33] Wilsbacher L, McNally EM. Genetics of cardiac developmental disorders: cardiomyocyte proliferation and growth and relevance to heart failure. Annu Rev Pathol 2016;11:395–419.
[34] Sedmera D, Pexieder T, Vuillemin M, Thompson RP, Anderson RH. Developmental patterning of the myocardium. Anat Rec 2000;258(4):319–37.
[35] Klaassen S, Probst S, Oechslin E, Gerull B, Krings G, Schuler P, et al. Mutations in sarcomere protein genes in left ventricular noncompaction. Circulation 2008;117(22):2893–901.
[36] Dellefave LM, Pytel P, Mewborn S, Mora B, Guris DL, Fedson S, et al. Sarcomere mutations in cardiomyopathy with left ventricular hypertrabeculation. Circ Cardiovasc Genet 2009;2(5):442–9.
[37] Towbin JA, Lorts A, Jefferies JL. Left ventricular non-compaction cardiomyopathy. Lancet 2015;386(9995):813–25.
[38] Sanger JM, Wang J, Gleason LM, Chowrashi P, Dube DK, Mittal B, et al. Arg/Abl-binding protein, a Z-body and Z-band protein, binds sarcomeric, costameric, and signaling molecules. Cytoskeleton 2010;67(12):808–23.
[39] Kioka N, Ueda K, Amachi T. Vinexin, CAP/ponsin, ArgBP2: a novel adaptor protein family regulating cytoskeletal organization and signal transduction. Cell Struct Funct 2002;27(1):1–7.
[40] Wang B, Golemis EA, Kruh GD. ArgBP2, a multiple Src homology 3 domain-containing, Arg/Abl-interacting protein, is phosphorylated in v-Abl-transformed cells and localized in stress fibers and cardiocyte Z-disks. J Biol Chem 1997;272(28):17542–50.
[41] Takasaki A, Hirono K, Hata Y, Wang C, Takeda M, Yamashita JK, et al. Sarcomere gene variants act as a genetic trigger underlying the development of left ventricular noncompaction. Pediatr Res 2018;84(5):733–42.
[42] Heling A, Zimmermann R, Kostin S, Maeno Y, Hein S, Devaux B, et al. Increased expression of cytoskeletal, linkage, and extracellular proteins in failing human myocardium. Circ Res 2000;86(8):846–53.
[43] Tagawa H, Wang N, Narishige T, Ingber DE, Zile MR, Gt Cooper. Cytoskeletal mechanics in pressure-overload cardiac hypertrophy. Circ Res 1997;80(2):281–9.